In situ analysis of Refractory Metal Nuggets in carbonaceous chondrites

Luke Daly[a,*], Phil A. Bland[a], Kathryn A. Dyl[a], Lucy V. Forman[a], Katy A. Evans[a], Patrick W. Trimby[b], Steve Moody[b], Limei Yang[b], Hongwei Liu[b], Simon P. Ringer[c], Christopher G. Ryan[d], Martin Saunders[e]

[a]*Department of Applied Geology, Curtin University, GPO Box U1987, Perth, WA* 6845*, Australia.*
[b]*Australian Centre for Microscopy and Microanalysis and ARC Centre of Excellence for Design in Light Metals, The University of Sydney, NSW* 2006*, Australia.*
[c]*Australian Institute for Nanoscale Science and Technology, and School of Aerospace, Mechanical and Mechatronic Engineering, The University of Sydney, NSW,* 2006*, Australia.*
[d]*CSIRO Earth Sciences and Resource Engineering,* 26 *Dick Perry Avenue, Kensington, Perth, WA* 6151*, Australia.*
[e]*Centre for Microscopy, Characterisation and Analysis, The University of Western Australia, WA* 6009*, Australia.*

Abstract

Micrometre to sub-micrometre scale alloys of platinum group elements (PGEs) know as refractory metal nuggets (RMNs) have been observed in primitive meteorites. The Australian Synchrotron X-ray Fluorescence (XRF) beamline, in tandem with the Maia detector, allows rapid detection of PGEs in concentrations as low as 50-100 ppm at 2 µm resolution. Corroborating this analysis with traditional electron microscopy techniques, RMNs can be rapidly identified *in situ* within carbonaceous chondrites. These results dispute the assumption of previous studies: that RMNs are unique to Ca-Al-rich inclusions (CAIs). We find that RMNs are, in fact, observed within all components of carbonaceous chondrites, such as the matrix, chondrules, and sulphides (as well as CAIs). The chemistry of RMNs reveals a complex diversity of compositions, which nevertheless averages to CI chondrite abundances. This implies that RMNs are the dominant, if not sole host phase for PGEs. 109 RMNs from this study are combined with reported compositions in the literature, and compared to condensation models similar to Berg et al. (2009), RMNs derived experimentally by crystallisation (Schwander et al., 2015), host phase and host meteorite. This reveals only weak correlations between parent body processes (sulphidation) and nebular processes (condensation and crystallisation) with RMN compositions. It appears that none of these processes acting in isolation or in tandem can explain the diversity we observe in the RMN population. Our interpretation is that the Solar Nebula inherited an initially compositionally diverse population of RMNs from the giant molecular cloud; that a variety of Solar System processes have acted on that population; but none have completely homogenised it. Most RMNs have experienced disk and asteroidal processing, but some may have retained a primordial composition. RMNs have been identified in pre-solar graphite (Croat et al., 2013) grains. We anticipate that pre-solar RMNs will be present elsewhere in primitive meteorites.

Keywords: `Refractory Metal Nuggets, Solar Nebula, Solar System, Origin, Meteorites, carbonaceous chondrites`

*Corresponding author: Luke Daly, Email: luke.daly@postgrad.curtin.edu.au, telephone: +61497840194

1. Introduction

CAIs are the oldest solids to have formed in the solar system, with an age of 4567.30 ± 0.16 Ma (Connelly et al., 2012). CAIs have been interpreted as primary high temperature condensates, which formed close to the protosun during the initial stages of the Solar Nebula, although some inclusions experienced some degree of remelting (MacPherson et al., 2005). Analyses of CAIs indicate a significant enrichment in the PGEs W, Re, Os, Ir, Ru and Pt between 22.8-11.9 times the elemental abundance observed in carbonaceous Ivuna-type (CI) chondrites (Grossman, 1973; Wänke et al., 1974). This enrichment was predicted to manifest itself in the form of RMNs within these early condensates (Grossman & Ganapathy, 1976). This was confirmed by the observation of PGE-rich metal grains within CAIs in Allende (Palme & Wlotzka, 1976; Wark & Lovering, 1976).

Since this discovery, there has been ongoing debate over how RMNs formed. Palme & Wlotzka (1976) found the composition of the RMNs contained within a 20 µm CAI-hosted sulphide from Allende, plotted onto an ideal condensation curve for a nebular gas. The PGEs also had solar ratios as defined by CI chondrites. This suggested that these RMNs formed as homogeneous primary condensates in the Solar Nebula. However, these grains had also been affected by secondary alteration on the parent body, including oxidation, sulphurisation, and exsolution (Bischoff & Palme, 1987; Blum et al., 1988; Palme & Wlotzka, 1976). Furthermore, experimental results from Schwander et al. (2015) suggested that RMNs could form via separation of refractory metals from a CAI like liquid.

To ascertain whether such grains could be produced from condensation in the Solar Nebula, Grossman (1973) calculated the chemical composition of the solid phases that would condense from a cooling solar gas. This work has been developed and refined with more recent calculations for condensation in the Solar Nebula by Fegley & Palme (1985) and Lodders (2003). These studies indicated that the PGEs should condense between 1392 K and 1821 K in the form of RMNs. These predictions were supported by observations of sub-µm RMNs hosted within unaltered fluffy type A CAIs from Allende, with compositions consistent with a condensation origin, particularly the presence of elements such as Mo and W, which are easily lost with even minor degrees of alteration (Palme et al., 1998). These grains also exhibited none of the secondary alteration textures observed in previous studies (Blander et al., 1980; Eisenhour & Buseck, 1992).

It has also been postulated that RMNs could form outside the nebular as presolar grains (El Goresy et al., 1977; Wark & Lovering, 1976), due to observed varying abundances of PGEs within isolated RMNs hosted within CAIs, when compared to CI ratios (Wark & Lovering, 1976). With recent work suggesting a mechanism of formation of pre-solar-RMNs in asymptotic giant branch stars (Schwander et al., 2014b), following the observation of RMNs found within pre-solar graphite (Croat et al., 2013).

Further analysis of RMNs divided them into two distinct families within CAIs (El Goresy et al., 1978); large 1-1000 µm multiphase inclusions containing micrometre-sized grains of RMNs (Blum et al., 1988), and isolated micrometre to sub-micrometre RMNs (Wark, 1986). Studies by El Goresy et al. (1977) and El Goresy et al. (1978) suggested that RMNs in multiphase inclusions had non-solar abundances of PGEs

and that isolated RMNs had solar abundances, therefore indicating, alongside the condensation sequence of minerals which hosted the multiphase inclusions, that they could have had a pre-solar origin and the isolated grains may have had a nebular origin. However, subsequent analysis of the RMNs described by Palme & Wlotzka (1976) and Wark & Lovering (1976) showed that exsolution, oxidation and sulphurisation textures were present. This implied that the grains were affected by parent body processes that remobilised the PGEs, and therefore they cannot be considered as primary nebular condensates (Bischoff & Palme, 1987; Blum et al., 1988).

The analysis of RMNs has been limited by the difficulty of finding sufficient numbers due to their small size. This has meant that the contextual work on RMNs has been restricted to CAIs. Anders et al. (1975) noted that PGEs were enriched in residue samples of Allende (CV3oxA) that have been dissolved with strong acids. This observation prompted Berg et al. (2009) to study similar residues from the Murchison (CM2) meteorite. Their procedure concentrated RMNs and permitted the analysis of several hundred grains rather than the < 20 analysed *in situ* in CAIs from previous studies. Following earlier work, Berg et al. (2009) proceeded with the assumption that RMNs in their residues had previously been associated with CAIs. The compositions of RMNs contained within these residues from energy-dispersive x-ray spectroscopy (EDS) were in agreement with theoretical equilibrium condensation calculations for similar grains (Campbell et al., 2001), this led Berg et al. (2009) to conclude that all the analysed grains were nebula condensates. However, later work by Schwander et al. (2014a) on RMNs from Murchison, Allende and Leoville, show that some but not all RMNs from these residues have been affected by metamorphic oxidation and sulphidation on the parent body resulting in the loss of W and Mo.

The abundant grains found in acid residues have significantly expanded the number of analyses of RMNs, but the loss of contextual information during acid dissolution of the bulk sample severely limits interpretation of the data. The assumption that has arisen in prior studies is that RMNs are unique to CAIs (Berg et al., 2009; Bischoff & Palme, 1987; Blander et al., 1980; Eisenhour & Buseck, 1992; El Goresy et al., 1978; Fegley & Kornacki, 1984; Grossman et al., 1977; Palme & Wlotzka, 1976; Palme et al., 1982; Sylvester et al., 1990; Wark, 1986; Wark & Lovering, 1976) with one exception: recent work by Croat et al. (2013) described RMNs contained within pre-solar graphite. These are the only RMNs that can be interpreted as having a pre-solar origin with relative certainty.

A diversity of terms can be found in the literature applied to these materials. In this study we will adopt the following terminology: RMNs will refer to any micrometre-sub micrometre metal alloy grain that contains > 1 wt% of any PGE (Re, Os, Ir, Pt, Ru, Rh, Pd, W, or Mo). If there is sufficient evidence to suggest a mechanism for how the RMN formed, a suitable precursor shall be attached to the start of the word i.e. presolar-RMN for an RMN with a demonstrably presolar origin similar to the naming scheme adopted by Croat et al. (2013). This can be extended to any process e.g. sulphidation would produce sulphidation-RMNs, and primary nebular condensates would be designated condensation-RMNs etc.

This paper presents a multidisciplinary study using the Australian Synchrotron (AS) XRF beamline

alongside scanning electron microscopy (SEM) with EDS to facilitate rapid identification of RMNs *in situ*. The applications of these techniques allow rapid non-destructive quantification and determination at sub-micrometre scales whilst preserving context. The results of these analyses call into question the assumption that RMNs are unique to CAIs: we observe them in many chondritic components, and when they are compared to condensation models also call into question the idea that a large fraction of RMNs formed via condensation and our assumptions about the conditions and processes prevalent at the start of the Solar Nebula.

2. Method

The samples analysed in this study are the primitive carbonaceous chondrites: C2- ungrouped Acfer 094, C2-ungrouped Adelaide, CO3.0 ALH77307, CV3 Allende, CR2 Kaidun, CR2 Renazzo, and CV2 Vigarano.

2.1. X-Ray Fluorescence Microscopy

The samples were analysed using the XRF Beamline at the AS, combined with the Maia detector; a custom made 384 Si-diode detector (Ryan et al., 2010) with a dwell time of 0.488 msec per pixel. A more detailed discussion of the technique and its application to meteorites can be found in (Dyl et al., 2014). This technique allows for rapid data collection over large areas with a resolution of 2 µm. The detector can analyse elements between the 4-18 keV range (Ryan et al., 2010). A particularly useful detail for this study is that PGE Lα, β, and γ energy peaks for Os, Ir and Pt lie in the most sensitive region of the spectrum (Figure 1), with L-alpha peaks at 8.910, 9.174 and 9.441 keV respectively (Dyl et al., 2014), which permits detection down to 50-100 ppm for these elements (Cleverley et al., 2012).

The data collected is interpreted using the GeoPIXE software, which uses a dynamic analysis matrix to deconvolve peaks of each individual element to generate elemental distribution maps (Ryan et al., 1995). The element maps are used to identify pixel-sized hotspots of PGEs as likely candidates for the location of RMNs with slight adjustments to contrast and brightness to make the most abundant regions stand out from the background.

The sample of Acfer 094 had been gold coated for previous studies and, although this has been largely removed, a small residue remains. This generates a slight problem as the gold peak is in the same region of the spectrum as the Os, Ir, Pt energy peaks and swamps the spectrum, generating false positives. In the case of this sample, the problem was countered by analysing each spectrum on an individual basis to ensure true RMNs were observed and not a residual gold particle from a previous coat.

Due the penetrating nature of the hard X-ray beam employed (18.5 keV), fluorescence X-rays from elements are received from up to 100 µm depth into the sample (Dyl et al., 2014). This generates a problem when trying to corroborate PGE hotspots with established techniques such as SEM and EDS, which only have penetration depths of $\sim$ 1 µm. This, coupled with the size of the RMNs, which tend to be 90 nm-1.2 µm (Berg et al., 2009) means that any one PGE hotspot identified with the synchrotron has a 99% chance

of being buried beneath the surface of the sample. However, it is also a benefit as a larger number of *in situ* grains are observed.

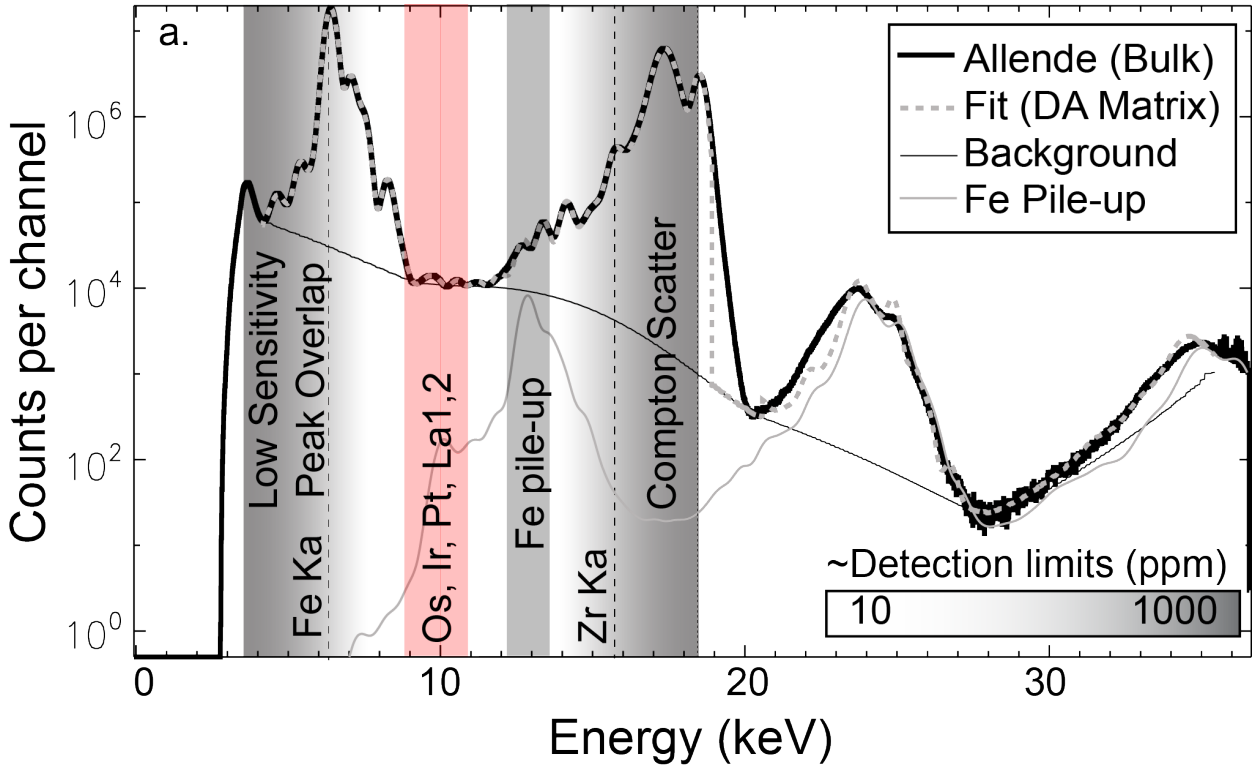

Figure 1: Bulk Synchrotron spectrum from Allende; with the raw data depicted by the bold line and the fit calculated by GeoPIXE^{TM} indicated by the dashed line. The solid and thinner black line signifies the background contribution to the spectra. Taking into account contributions such as the large iron peak and secondary pile up peak, along with the Compton scatter region, the detection limits are highlighted by the greyscale gradient map. The location of the Lα peaks for Os, Ir and Pt are highlighted in red and sit in the region of highest sensitivity and lowest detection limits. Image adapted after Dyl et al. (2014).

2.2. Scanning Electron Microscopy:

The samples were analysed using two instruments; the Zeiss 1555 VP-FESEM at the Centre for Microscopy, Characterisation and Analysis (CMCA), University of Western Australia, and the Zeiss EVO50 LaB6 at the Australian Centre for Microscopy and Microanalysis (ACMM), Sydney, both equipped with 80 mm^2 high count rate silicon drift detector (SDD) EDS detectors. In both cases an accelerating voltage of 25 kV was used. Element maps derived from the AS data are geo-referenced with the live SEM image using the image overlay feature in Oxford Instruments AZtec software. This method allowed rapid searching for RMNs present at the surface of the sample with high accuracy. This process was augmented by the feature mapping software in the Inca suite, which allowed whole thin section searches based on contrast bands. As RMNs are one of the densest phases in meteorites and backscatter microscopy reveals density differences in mineral phases, the brightest spots were refractory metal grains. This allowed us to analyse every metal grain at the

surface of a sample. Metal alloys containing PGEs were re-found and more detailed EDS was undertaken. This method found all the RMNs that were found using the combined synchrotron and EDS geo-referencing technique described above, along with a few others that were missed. The composition of the grains was derived using standardless quantitative analysis, using the standard database embedded within the AZtec software. This resulted in a total of 195 RMNs, however, the EDS spectra obtained through the feature mapping technique does not produce quantitative compositions. 109 RMNs were re-found in the sample and a second EDS measurement was taken with longer dwell times to produce more reliable compositional measurements.

Some RMNs were extracted from the sample using a Focussed Ion Beam (FIB) techniques using the Zeiss Auriga FIB-SEM at the ACMM, Sydney. A thin protection layer of platinum was deposited using secondary electrons followed by a much thicker platinum layer deposited using gallium ions. The sample was then cut out using the gallium beam and extracted using a Kleindiek micromanipulator and welded to a copper transmission electron microscopy (TEM) mount by depositing more platinum. The sample was thinned down to 100 nm using a fine Gallium beam. The samples were analysed using Transmission Kikuchi diffraction (TKD) on a Zeiss ULTRA Plus FEG SEM at the ACMM, Sydney. TKD mapping was performed using a Nordlys-NANO EBSD detector, and EDS maps were collected with an X-Max 20 mm^2 SDD EDS detector using an acceleration voltage of 30 kV.

2.3. Condensation model and crystallisation proxy

An exhaustive literature search was conducted in an attempt to produce a library of all previous RMN compositional data (Berg et al., 2009; Bischoff & Palme, 1987; Blander et al., 1980; Wark & Lovering, 1976; Wark, 1986; Palme et al., 1982; Croat et al., 2013; Schwander et al., 2014a; Palme et al., 1994; Wark & Lovering, 1978; Harries et al., 2012). We also include compositions of RMNs thought to be derived from crystallisation processes (Schwander et al., 2015; Rudraswami et al., 2014). These analyses were plotted alongside observed RMN compositions from this study.

Compositions of RMNs have been corrected removing elements present in the surrounding host phase and only retaining elements present in RMNs: Fe, Ni, Ru, Rh, Mo, W, Re, Os, Ir, and Pt (Harries et al., 2012). It should be noted that Fe may be slightly underestimated due to small amounts of Fe in the surrounding phases, diluting the Fe signal. RMNs compositions were converted to atomic percent (at%) and renormalised. Compositions for hypothetical RMN condensates were calculated using the approach described in Palme & Wlotzka (1976). Oxide compounds were neglected and all activity coefficients were set to 1, in accordance with other condensation models. Temperatures were calculated for analysed RMNs using a least squares fit for each RMN composition to the predicted RMN composition as a function of temperature for pressures 10^{-3} bar and 10^{-4} bar. The results of Harries et al. (2012) were used as a check for the method and were found to be generally consistent with the results obtained in this model.

3. Results

3.1. Synchrotron

In depth analyses of the element maps derived from the AS were used to target and identify hotspots of PGEs. The vast majority of observed hotspots are pixel-sized, indicating grains are < 2 µm. Each carbonaceous chondrite section analysed yielded an average of 10 hotspots per sample, with a maximum of 70 in Vigarano and a minimum of two in Adelaide and Acfer 094. The proximity of the Kα and Lα peaks of the PGEs to each other and major elements such as Zn, combined with the penetration depth, make it difficult to deconvolve the spectrum into individual element peaks. This means that the spectrum's shape is defined by the most abundant element in that energy range. Great care was taken in analysing the spectra to avoid misidentification due to peak overlaps, removing false positives. Most hotpots observed are located within CAIs as expected, however a number are observed within chondrules, sulphides, and matrix (Table 1).

Table 1: RMNs identified by synchrotron.

Meteorite	Total RMNs	Host		
		CAI	Chondrule	Matrix
Acfer	2	0	1	1
Adelaide	2	1	0	1
ALH 77307	17	12	0	5
Kaidun	9	0	1	8
Renazzo	6	0	2	4
Vigarano	71	69	2	0

3.2. Synchrotron to SEM

Table 2: RMN hosts from SEM analysis and EDS.

Meteorite	Total RMNs	Host			
		Chondrule	Matrix	Sulphide	CAI
Adelaide	2	1	0	0	1
ALH 77307	18	0	4	5	9
Allende	103	3	6	65	29
Murchison	2	0	0	0	2
Vigarano	36	1	0	19	16

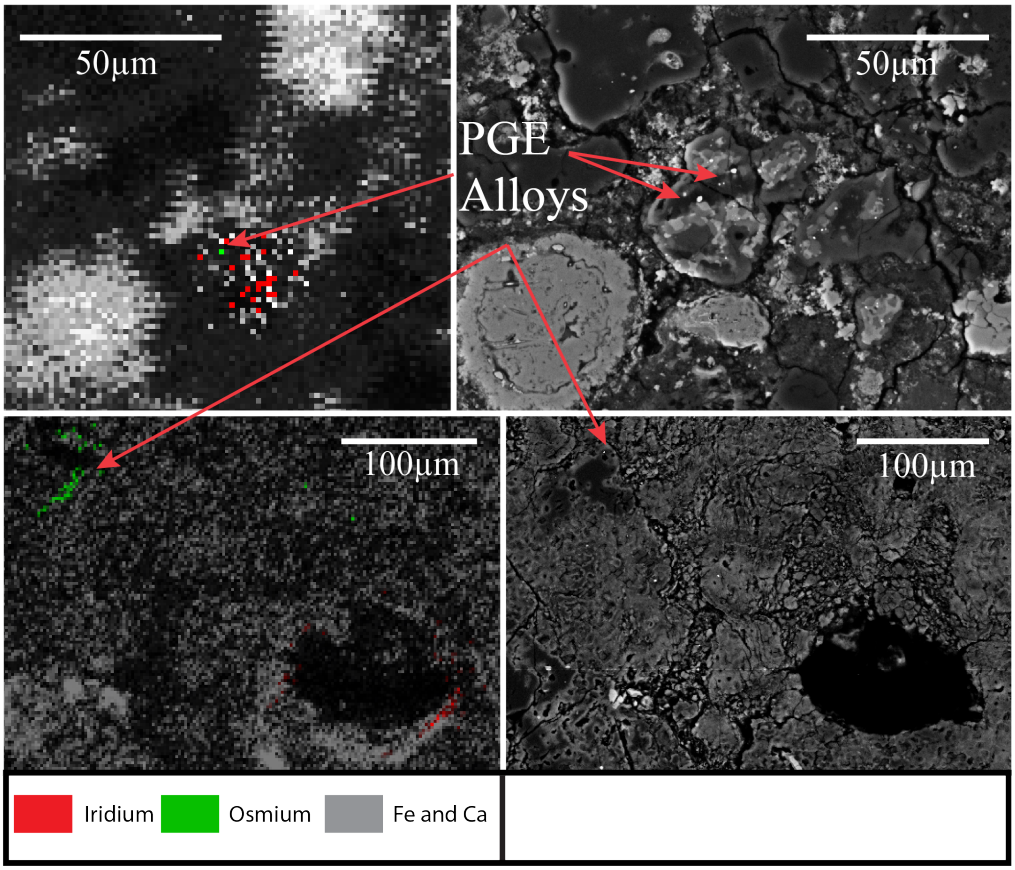

Figure 2: Synchrotron maps (left hand side) and corresponding regions in backscattered electron images from the SEM (right hand side) showing PGE hotspots in synchrotron data (Ir in red and Os in green) relate to RMN localities on the surface of the thin section (bright points).

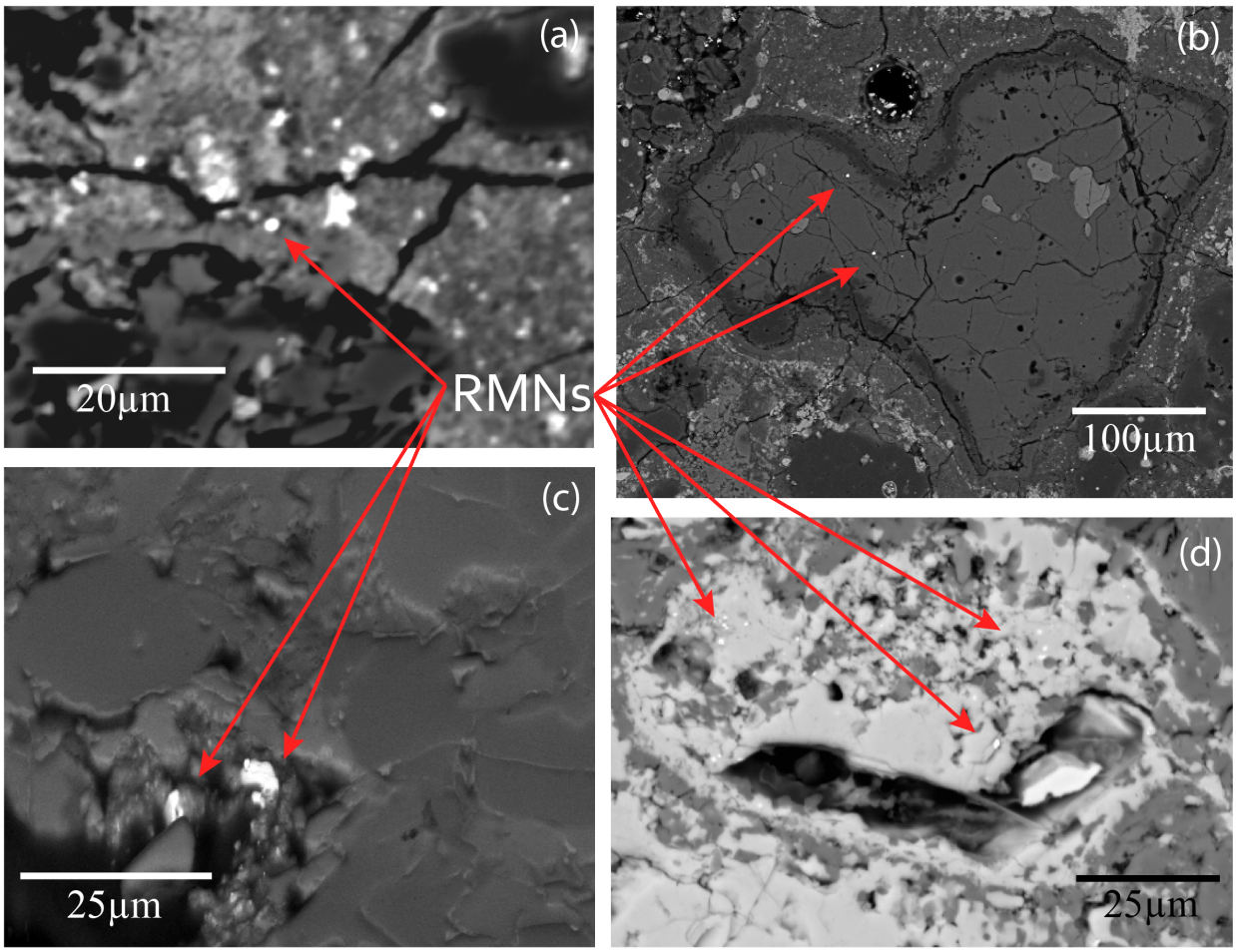

Figure 3: SEM backscatter images of RMNs in all meteoritic components a) RMN hosted in matrix from ALH 77307 b) RMN hosted in a CAI in ALH 77307, c) RMN hosted in a Chondrule in Allende d) RMNs hosted within a sulphide rim in Allende.

Despite the low probability of observing RMNs at the surface when comparing the Synchrotron and EDS data sets, 195 RMNs were confirmed and identified using the image overlay technique and feature mapping (Figure 2). These RMNs vary in size from 0.1 µm to 9.71 µm with an average of 1.7 µm, across several meteorite samples; 2 in Adelaide, 103 in Allende, 36 in Vigarano, and 18 in ALH 77307. Not all Synchrotron PGE hotspots yielded a RMN however some hotspots revealed more than one. The feature mapping technique also increased the number of observed RMNs, revealing some that the Synchrotron data had not identified; hence, the disparity between the number of PGE hotspots found with the Synchrotron and the SEM. Most RMNs are found in CAIs (57) or sulphides hosted within CAIs, chondrules, and chondrule rims (89), but a number are observed within the matrix (10) and chondrules (5) of these meteorites (Figure 3)(Table 2). Of the 195 RMNs identified 109 have reliable chemical analyses. The composition of the RMNs derived from EDS varies greatly between host and samples; Re, and Rh were below detection limits for most RMNs analysed. The compositions of RMNs observed within each component are summarised in Table 3 and average compositions of RMNs in each component are detailed in Table 4.

Table 3: RMN compositions from EDS (at%))

Meteorite	Host	Fe	Ni	Ru	Rh	Mo	W	Re	Os	Ir	Pt
Adelaide	CAI	66.91	7.68	7.01	0.00	14.10	0.00	0.00	0.00	0.00	4.29
Adelaide	Chondrule	91.83	2.56	2.42	0.00	0.00	0.00	0.00	1.26	0.95	0.99
ALH 77307	CAI	25.87	2.05	13.70	0.00	21.02	2.62	0.00	14.24	20.51	0.00
ALH 77307	CAI	43.02	3.41	13.87	0.00	16.69	0.00	0.00	9.47	13.54	0.00
ALH 77307	CAI	55.54	9.42	7.51	0.00	6.68	0.00	0.00	6.97	4.02	9.85
ALH 77307	CAI	46.34	6.68	13.07	3.19	14.82	0.00	0.00	4.65	2.94	8.31
ALH 77307	CAI	40.05	3.78	9.12	0.00	38.79	2.04	0.00	2.78	1.42	2.01
ALH77307	CAI	50.92	4.22	6.30	0.00	26.59	1.79	0.00	7.93	2.24	0.01
Allende	CAI	58.52	2.73	10.85	0.00	17.39	0.00	0.00	4.33	6.18	0.00
Allende	CAI	46.38	13.56	14.97	0.00	0.00	0.00	0.00	7.71	12.91	4.48
Allende	CAI	16.08	29.20	14.37	0.00	24.33	0.00	0.00	4.98	5.77	5.27
Allende	CAI	44.52	0.00	13.42	0.00	22.77	0.00	0.00	9.11	10.19	0.00
Allende	CAI	79.26	0.00	20.74	0.00	0.00	0.00	0.00	0.00	0.00	0.00
Allende	CAI	58.84	3.86	6.20	0.00	13.62	1.42	0.81	5.89	9.35	0.00
Allende	CAI	41.85	4.48	7.43	0.00	20.26	2.85	0.81	8.35	13.95	0.00
Allende	CAI	47.35	4.18	7.03	0.00	18.33	2.44	0.81	7.33	12.53	0.00
Allende	CAI	63.74	5.70	5.92	0.00	16.37	0.86	0.00	2.89	4.53	0.00
Allende	CAI	18.05	0.00	44.55	0.00	0.00	0.00	0.00	22.65	14.76	0.00
Allende	CAI	35.26	5.53	26.25	0.00	0.00	0.00	0.00	18.75	14.20	0.00

Table 3 – continued from previous page

Meteorite	Inclusion	Fe	Ni	Ru	Rh	Mo	W	Re	Os	Ir	Pt
Allende	CAI	21.75	1.29	43.16	0.00	0.00	0.00	0.00	16.93	16.87	0.00
Allende	CAI	20.31	0.00	45.65	0.00	0.00	0.00	0.00	16.45	17.59	0.00
Allende	CAI	54.27	6.36	17.83	0.00	0.00	0.00	0.00	10.49	11.05	0.00
Allende	CAI	21.28	5.37	41.05	0.00	6.00	0.00	0.00	12.41	13.90	0.00
Allende	CAI	30.33	12.02	31.13	0.00	2.69	0.00	0.00	10.17	13.65	0.00
Allende	CAI	62.02	0.00	19.07	0.00	2.42	0.00	0.00	8.99	7.51	0.00
Allende	CAI	26.96	2.91	31.38	0.00	16.97	0.00	0.00	11.37	10.40	0.00
Allende	CAI	49.36	3.57	15.59	0.00	16.21	0.00	0.00	7.13	8.14	0.00
Allende	CAI	21.49	9.69	38.72	0.00	0.00	0.00	0.00	16.43	13.67	0.00
Allende	CAI	30.89	24.92	22.90	0.00	0.00	0.00	0.00	10.80	10.48	0.00
Allende	CAI	37.46	49.53	4.20	0.00	0.00	0.00	0.00	1.45	7.37	0.00
Allende	CAI	29.81	20.46	28.26	0.00	0.00	0.00	0.00	10.64	10.83	0.00
Allende	CAI	33.96	31.63	16.94	0.00	0.00	0.00	0.00	7.19	10.28	0.00
Allende	CAI	30.61	1.92	64.68	0.00	0.00	0.00	0.00	0.50	2.29	0.00
Allende	CAI	39.67	42.65	5.07	0.00	0.00	0.00	0.00	3.81	7.12	1.67
Allende	Chondrule	32.36	64.36	0.47	0.00	0.00	0.00	0.00	0.00	0.60	2.20
Allende	Chondrule	34.61	62.56	0.00	0.00	0.00	0.00	0.00	0.00	1.05	1.77
Allende	Chondrule	29.73	32.69	28.56	0.00	0.00	0.00	0.00	6.45	1.58	0.99
Allende	Matrix	51.42	46.51	0.00	0.00	0.00	0.00	0.00	0.74	0.00	1.33
Allende	Matrix	40.64	58.35	0.00	0.00	0.00	0.00	0.00	0.22	0.36	0.43
Allende	Matrix	48.94	47.23	1.73	0.00	0.00	0.00	0.00	0.51	0.61	0.99
Allende	Matrix	74.55	21.37	1.32	0.00	0.00	0.00	0.00	0.56	0.97	1.23
Allende	Matrix	60.72	38.52	0.00	0.00	0.00	0.00	0.00	0.00	0.00	0.76
Allende	Matrix	66.28	33.48	0.00	0.00	0.00	0.25	0.00	0.00	0.00	0.00
Allende	Sulphide	62.38	27.79	0.00	0.00	0.00	0.00	0.00	0.00	2.04	7.79
Allende	Sulphide	61.34	32.82	0.00	0.00	0.00	0.00	0.00	0.00	0.00	5.84
Allende	Sulphide	62.18	30.78	0.00	0.00	0.00	0.00	0.00	0.00	6.12	0.92
Allende	Sulphide	45.18	33.51	0.00	0.00	0.00	0.00	0.00	0.00	1.76	19.55
Allende	Sulphide	45.41	32.25	0.00	0.00	0.00	0.00	0.00	0.66	4.83	16.84
Allende	Sulphide	51.91	31.75	0.00	0.00	0.00	0.00	0.00	0.00	6.68	9.66
Allende	Sulphide	28.97	63.65	0.00	0.00	0.00	0.00	0.00	0.00	7.38	0.00
Allende	Sulphide	43.49	34.23	0.00	0.00	0.00	0.00	0.00	0.00	5.97	16.30
Allende	Sulphide	68.86	28.60	0.00	0.00	0.00	0.00	0.00	0.00	0.00	2.54
Allende	Sulphide	71.52	27.73	0.00	0.00	0.00	0.00	0.00	0.00	0.00	0.75

Table 3 – continued from previous page

Meteorite	Inclusion	Fe	Ni	Ru	Rh	Mo	W	Re	Os	Ir	Pt
Allende	Sulphide	65.89	29.19	0.00	0.00	0.00	0.00	0.00	0.00	0.76	4.15
Allende	Sulphide	71.20	26.74	0.00	0.00	0.00	0.00	0.00	0.25	0.34	1.48
Allende	Sulphide	69.98	25.46	0.00	0.00	3.71	0.00	0.00	0.85	0.00	0.00
Allende	Sulphide	71.78	26.60	0.00	0.00	0.00	0.00	0.00	0.00	0.00	1.62
Allende	Sulphide	84.18	11.12	0.00	0.00	3.40	0.00	0.00	0.00	0.00	1.30
Allende	Sulphide	66.35	30.63	0.00	0.00	0.00	0.00	0.00	0.00	0.00	3.02
Allende	Sulphide	70.86	28.62	0.00	0.00	0.00	0.00	0.00	0.00	0.00	0.53
Allende	Sulphide	68.70	28.19	0.00	0.00	0.00	0.00	0.00	0.00	0.00	3.11
Allende	Sulphide	68.48	28.34	0.00	0.00	0.00	0.00	0.00	0.23	0.51	2.43
Allende	Sulphide	69.80	28.88	0.00	0.00	0.00	0.00	0.00	0.00	0.00	1.32
Allende	Sulphide	67.39	30.42	0.00	0.00	0.00	0.00	0.00	0.00	0.00	2.19
Allende	Sulphide	73.45	26.11	0.00	0.00	0.00	0.00	0.00	0.00	0.00	0.44
Allende	Sulphide	70.70	28.98	0.00	0.00	0.00	0.00	0.00	0.00	0.00	0.32
Allende	Sulphide	44.07	3.14	0.00	0.00	0.00	0.00	1.39	49.08	2.33	0.00
Allende	Sulphide	44.09	40.81	0.00	0.00	0.00	0.00	0.00	0.00	6.02	9.08
Allende	Sulphide	57.77	35.29	0.00	0.00	0.00	0.00	0.00	0.00	4.11	2.83
Allende	Sulphide	60.14	34.86	0.00	0.00	0.00	0.00	0.00	0.00	2.60	2.40
Allende	Sulphide	63.53	29.87	0.00	0.00	0.00	0.00	0.00	5.80	0.80	0.00
Allende	Sulphide	42.84	41.51	0.00	0.00	0.00	0.00	0.00	0.00	2.21	13.45
Allende	Sulphide	49.13	48.16	0.00	0.00	0.00	0.00	0.00	0.00	1.80	0.91
Allende	Sulphide	49.27	37.48	0.00	0.00	0.00	0.00	0.00	0.00	1.39	11.86
Allende	Sulphide	46.23	40.47	0.00	0.00	0.00	0.00	0.00	0.00	2.60	10.70
Allende	Sulphide	49.61	31.37	0.00	0.00	0.00	0.00	0.00	0.00	2.32	16.70
Allende	Sulphide	39.10	46.71	0.00	0.00	0.00	0.00	0.00	0.00	3.33	10.85
Allende	Sulphide	51.00	33.81	0.00	0.00	0.00	0.00	0.00	0.00	3.55	11.64
Allende	Sulphide	62.56	34.51	0.00	0.00	0.00	0.00	0.00	0.00	1.34	1.59
Allende	Sulphide	71.25	23.25	0.00	0.00	0.00	0.00	0.00	0.00	2.90	2.60
Allende	Sulphide	47.09	39.06	0.00	0.00	0.00	0.00	0.00	0.00	7.65	6.20
Allende	Sulphide	58.42	32.55	0.00	0.00	0.00	0.00	0.00	0.00	1.97	7.06
Allende	Sulphide	66.25	32.46	0.00	0.00	0.00	0.00	0.00	0.00	0.00	1.29
Allende	Sulphide	61.28	32.38	0.00	0.00	0.00	0.00	0.00	0.00	2.50	3.84
Allende	Sulphide	54.65	39.04	0.00	0.00	0.00	0.00	0.00	0.00	4.15	2.17
Allende	Sulphide	46.17	39.40	0.00	0.00	0.00	0.00	0.00	0.00	3.73	10.70
Allende	Sulphide	56.70	36.08	0.00	0.00	0.00	0.00	0.00	0.00	2.53	4.69

Table 3 – continued from previous page

Meteorite	Inclusion	Fe	Ni	Ru	Rh	Mo	W	Re	Os	Ir	Pt
Allende	Unknown	51.33	32.64	0.00	0.00	0.00	0.00	0.00	0.00	8.28	7.75
Murchison	CAI	57.29	5.14	5.26	0.00	24.25	1.58	0.00	3.61	1.49	1.39
Murchison	CAI	77.48	4.70	7.90	0.00	0.00	0.00	0.00	2.24	3.33	4.35
Murchison	Unknown	40.77	35.84	0.00	0.00	0.00	0.00	0.00	2.53	3.83	17.01
Murchison	Unknown	47.00	29.03	0.00	0.00	0.00	0.00	0.00	15.72	7.19	1.05
Murchison	Unknown	20.23	1.53	19.57	0.00	54.01	0.00	0.00	2.07	1.80	0.79
Vigarano	CAI	48.76	48.59	1.74	0.00	0.00	0.00	0.00	0.37	0.00	0.54
Vigarano	CAI	62.91	29.46	5.61	0.00	0.00	0.00	0.00	1.09	0.94	0.00
Vigarano	CAI	67.40	15.51	11.68	0.00	0.00	0.00	0.00	2.59	2.82	0.00
Vigarano	CAI	61.50	30.06	4.64	0.00	0.00	0.00	0.00	0.99	1.95	0.87
Vigarano	CAI	65.67	14.07	14.18	0.00	0.00	0.00	0.00	2.43	3.66	0.00
Vigarano	CAI	55.37	39.18	2.40	0.00	0.00	0.00	0.00	0.67	1.00	1.38
Vigarano	CAI	56.99	36.38	3.54	0.00	0.00	0.00	0.00	1.09	1.08	0.92
Vigarano	CAI	64.39	17.70	10.81	0.00	0.00	0.00	0.00	3.36	3.74	0.00
Vigarano	CAI	50.48	15.50	15.30	0.00	11.85	0.00	0.00	3.11	2.60	1.17
Vigarano	CAI	53.00	40.78	4.39	0.00	0.00	0.00	0.00	0.55	0.62	0.67
Vigarano	CAI	55.76	40.59	2.95	0.00	0.00	0.00	0.00	0.00	0.00	0.70
Vigarano	CAI	72.17	1.83	0.00	0.00	7.53	4.60	0.00	9.46	4.40	0.00
Vigarano	CAI	61.08	34.23	2.02	0.00	0.00	0.00	0.00	0.50	0.54	1.62
Vigarano	CAI	63.88	30.98	1.94	0.00	0.00	0.00	0.00	0.56	0.75	1.89
Vigarano	CAI	67.34	30.06	1.69	0.00	0.00	0.00	0.00	0.00	0.00	0.91
Vigarano	CAI	67.54	28.15	1.77	0.00	0.00	0.00	0.00	0.00	0.00	2.53
Vigarano	CAI	38.29	14.46	23.17	0.00	13.09	0.00	1.09	4.82	3.00	2.09

180

Table 4: Average RMN compositions by host (at%).

Inclusion	Fe	Ni	Ru	Rh	Mo	W	Re	Os	Ir	Pt
Average CAI	48.00	15.31	15.17	0.06	7.17	0.39	0.07	6.16	6.58	1.09
Average chondrule	47.13	40.54	7.86	0.00	0.00	0.00	0.00	1.93	1.05	1.49
Average matrix	57.09	40.91	0.51	0.00	0.00	0.04	0.00	0.34	0.32	0.79
Average sulphide	58.66	32.38	0.00	0.00	0.16	0.00	0.03	1.29	2.19	5.29
Average all RMNs	52.72	32.28	5.89	0.02	1.83	0.11	0.02	2.43	2.53	2.17

4. Discussion

4.1. Evaluation of the database

The removal of the host mineral phase composition from the RMN EDS measurement, resulted in small wt% totals. To evaluate whether the re-normalisation process has introduced any inherent biases or compound errors, each renormalised element was plotted in relation to the initial wt% total of PGEs + Fe + Ni before re-normalisation (Figure 4). If the normalisation process was producing a systematic error, steep trends from small wt% totals to high wt% totals would be observed. However, these graphs had very shallow to flat trends indicating normalisation has not introduced significant bias.

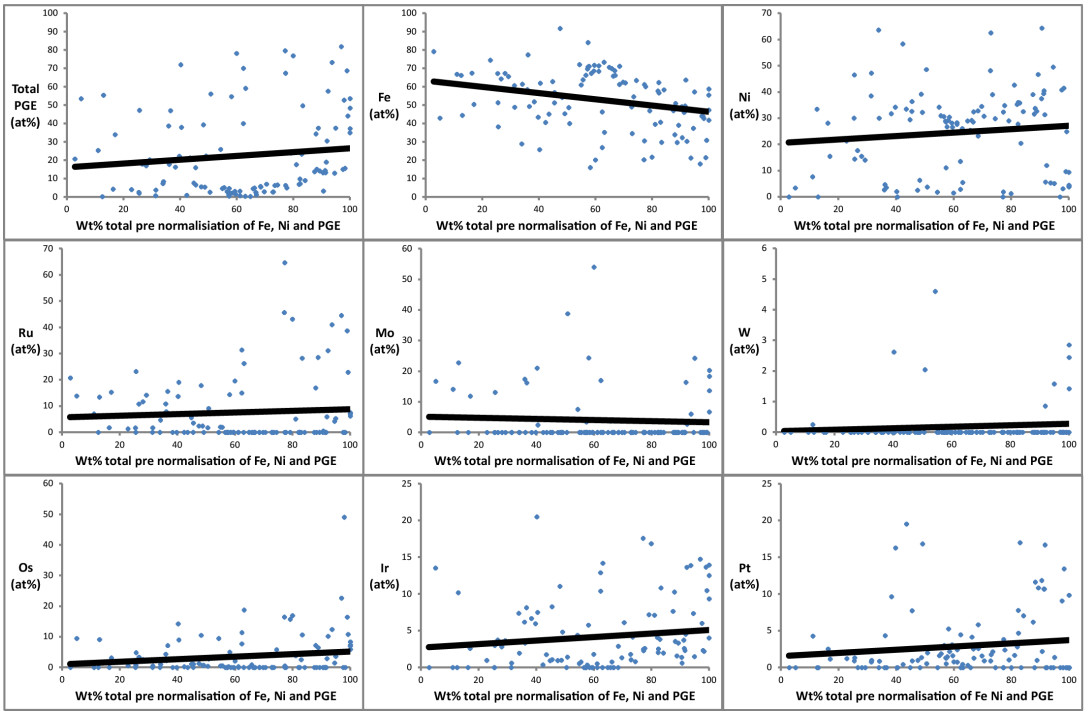

Figure 4: Graphs showing little variability between renormalised at% for each element on the y axis and the total wt% of all elements found in RMNs in the initial EDS measurement on the x axis.

4.2. RMNs within CAIs, chondrules and matrix:

Current theories surrounding the origin of RMNs are tied to their assumed unique occurrence within CAIs e.g. Berg et al. (2009). CAIs are high temperature condensates (Grossman & Ganapathy, 1976; Wänke et al., 1974) so the assumed model of formation for RMNs has been that they condensed at high temperatures in the same location and environment as CAIs (Grossman & Ganapathy, 1976). However, this single condensation event model is hard to reconcile with the myriad of compositions observed within RMNs (Grossman et al., 1977). In addition, it should be borne in mind that CAIs affect the bulk composition of meteorites by enhancing refractory abundance above CI, indicating that CAIs were added to an approximately solar bulk 'background' composition. But in chemical analysis of matrix, or (CAI-absent) CI chondrite, we still observe

PGEs. What then is the host phase of these elements? One possibility is finely comminuted CAI. However, if this were true, we would observe an enhancement in all refractory elements, which is not the case. The fact that we have now observed RMNs within matrix and chondrules demonstrates that CAIs are not a necessary factor in their formation. Indeed, their presence in chondritic components which formed at temperatures far below CAIs raises several new possibilities for RMN formation.

4.3. RMN compositional diversity

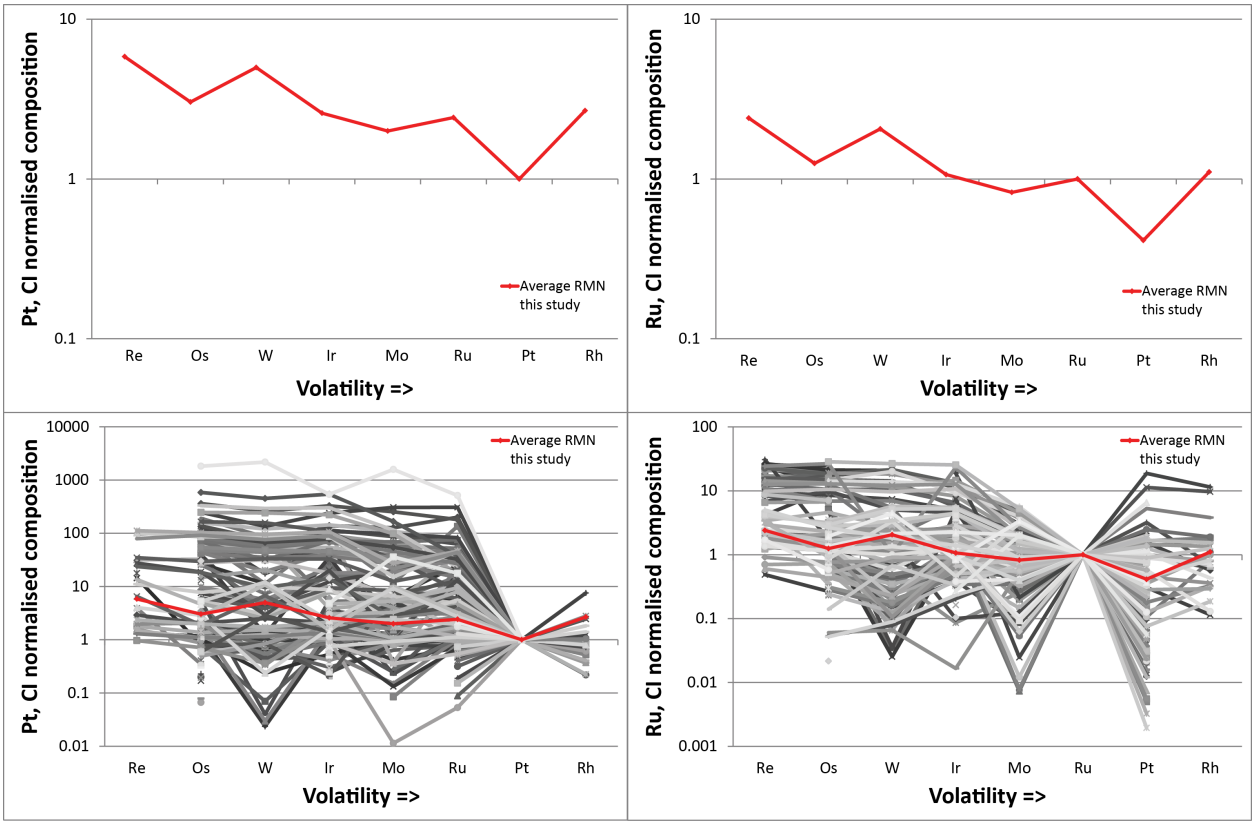

Figure 5: RMN compositions from this study, normalised to Pt then CI (left hand side) or Ru the CI (right hand side). Showing a wide range of individual RMN compositions (grey curves). However, the average RMN composition (red curve) has CI chondrite relative abundances for these elements

RMN PGE abundances compared to CI chondrite defined by (Lodders, 2003) (Figure 5) show large enrichments and depletions relative to CI, up to 1000x, for individual RMNs in this study. Most RMNs are equally enriched or depleted in all refractory elements, however, some RMNs have significant relative depletions in Mo and W. The RMNs associated with this trend are principally hosted within sulphides supporting the idea that sulphidation mobilises Mo and W (Palme et al., 1998). Nevertheless, the average RMN composition approximately follows a CI chondrite trend indicating that these refractory elements are primarily hosted within RMNs in meteorites.

The total PGE contents of RMNs when compared with Fe and Ni (Figure 6) reveal three main trends

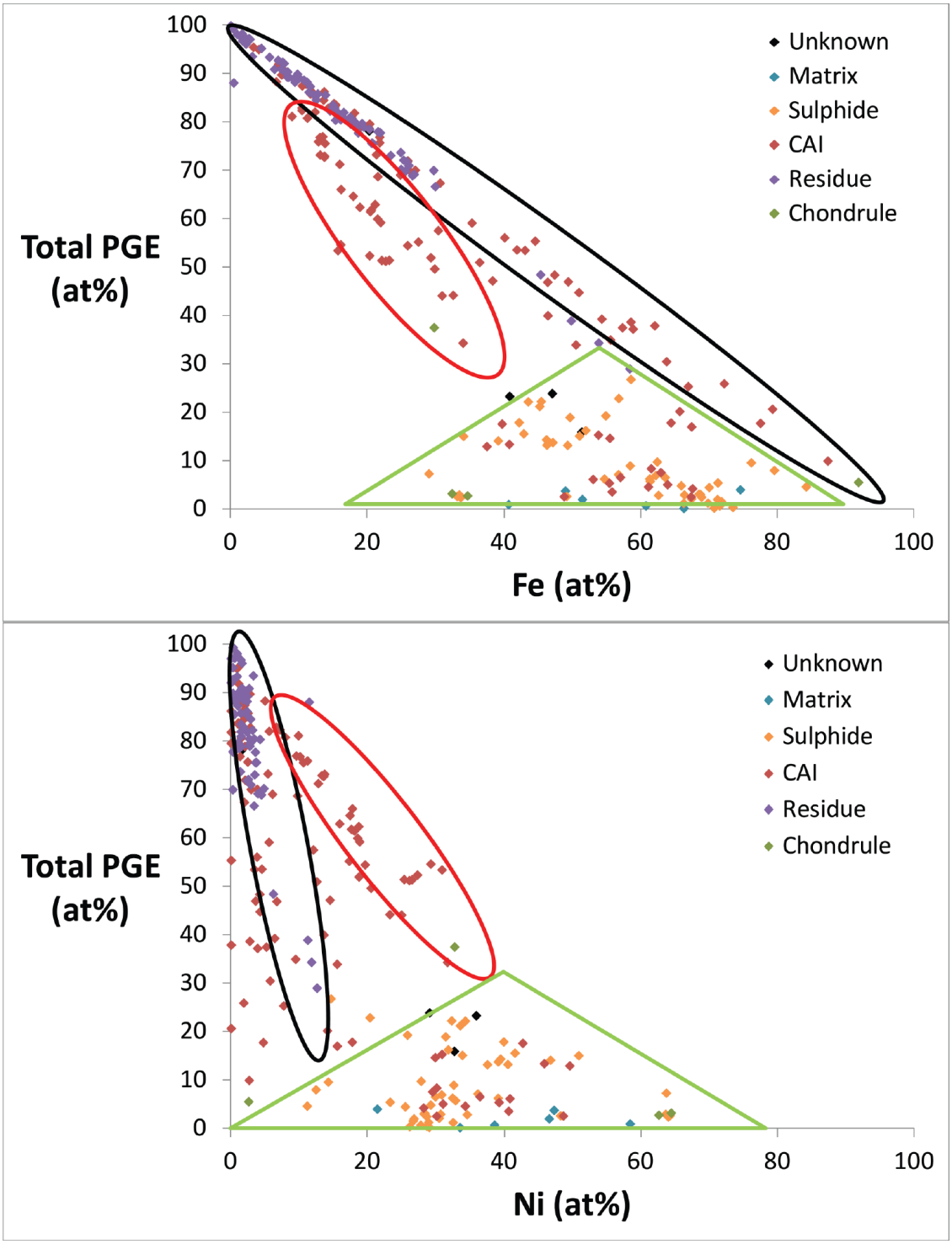

Figure 6: Total PGE vs Fe and total PGE vs Ni plots by host phase (this study and the literature) indicating a Fe mixing trend (black oval) and Ni mixing trend (red oval and a low PGE cluster (Green triangle) which is dominated by sulphide phases.

in the dataset: a Fe mixing line between 100 at% PGE and 100 at% Fe (black oval), a Ni mixing line from 80 at% PGE, 20 at% Fe to 30 at% PGE, 40 at% Fe (red oval,) and a 'low PGE region' PGE >30 at% and $30 - 80$ at% Fe (green triangle). RMNs found in acid residues are exclusively found within the high PGE portion of the Fe mixing line. The clustering of RMNs found within acid residues is likely to be a function of Berg et al. (2009) and Harries et al. (2012) preferentially selecting RMNs with high PGE abundances. It is probable that, if all residue RMNs were analysed, the full suite of RMN compositions would be revealed. The low PGE region is primarily composed of matrix, chondrule and sulphide hosted RMNs. CAI hosted RMNs are evenly spread across all regions. The universal presence of CAI hosted RMNs in all regions suggests that no single process homogenised the composition of RMNs within CAIs.

Furthermore the average chemical composition of RMNs within each host phase are significantly different (Table 4). Sulphide, matrix and chondrule hosted RMNs are depleted in most PGEs, relative to CAI hosted RMNs, and W and Mo are completely absent or in extremely low concentrations. There is a large range of RMN compositions observed within the data set. We will now compare the observed spread of RMN compositions to the compositional distribution expected to be produced by proposed RMN forming processes, specifically: condensation, crystallisation and sulphidation acting in isolation or in tandem.

4.3.1. Sulphidation as a RMN forming process

The high abundance of sulphide hosted RMNs contained within the low PGE region (Figure 6) potentially allows us to interpret RMNs within this region as derived from, or affected by, sulphidation. If we assume that sulphide hosted RMNs were formed or had their composition modified by sulphidation, then a parent body process has imposed a compositional fingerprint on these grains. It has been suggested that the presence of W and Mo could be used as an indicator for primitive RMNs as even low degrees of alteration that the RMNs experienced would remobilise these two elements (Eisenhour & Buseck, 1992). Therefore, the fact that no W or Mo are observed in sulphide-hosted RMNs may be taken as evidence that these grains have been altered. However, the presence of matrix, CAI and chondrule RMNs also within this region that are not associated with sulphides suggests that this region is not a unique expression of sulphidation and other processes can produce RMNs with low PGE abundances therefore the whole region cannot be explained by sulphidation.

4.3.2. Condensation as a RMN forming process

Calculated RMN condensation temperatures show a reasonable agreement with condensation models for some elements, particularly Fe and Mo. However, other elements, particularly Ni deviate from the expected curve by a substantial amount (Figure 7).

To evaluate how closely RMNs measured compositions agree with modelled compositions, RMNs were grouped where every element is within 5 at% or 15 at% agreement with the best fit calculated condensation composition (Figure 8). As the tolerance is raised from $5 - 15$ at% , the number of RMNs consistent with condensation models increases from 10% to 50%. These RMNs are clustered exclusively along the Fe mixing

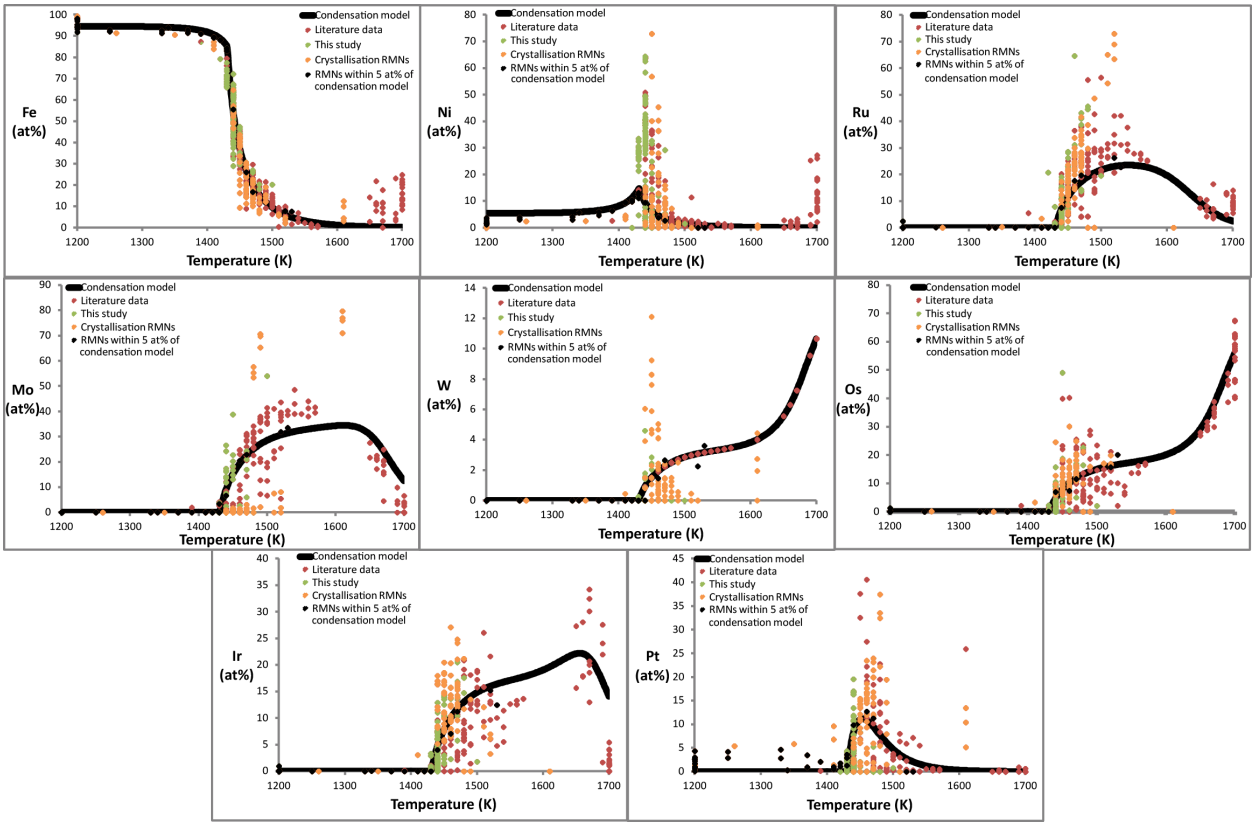

Figure 7: PGE abundance vs calculated condensation temperature at 10^{-4} bar for RMNs from this study, the literature and RMNs derived from crystallisation, indicating good correlations with Fe and Mo but very poor correlations with Ni and Ru

line. However, a significant portion of RMNs within the Fe mixing line do not conform to the condensation model even at high tolerance levels. This indicates that condensation is not exclusively responsible for RMNs within the Fe mixing line.

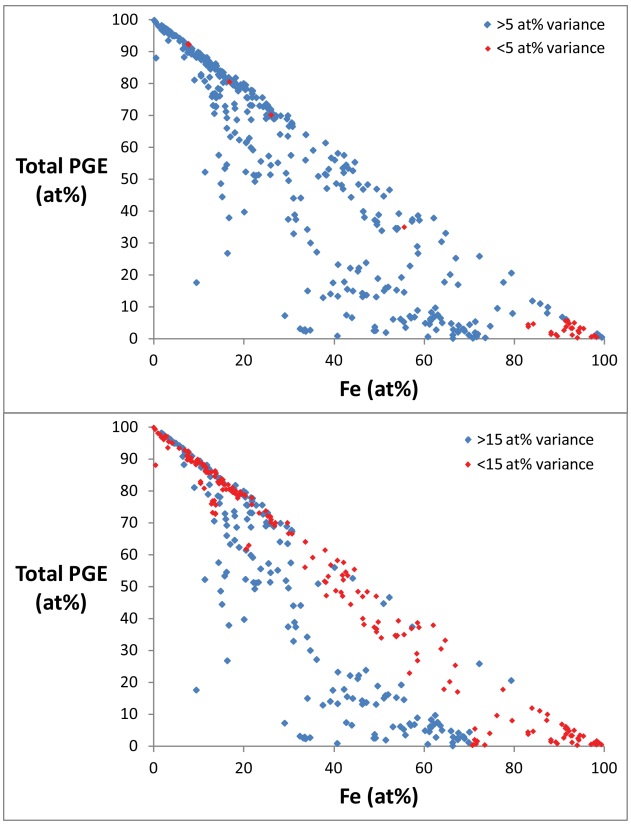

Figure 8: Total PGE vs Fe graphs showing RMNs within 5, and 15 at % tolerances of the condensation model in red

4.3.3. Crystallisation as a potential RMN forming process

Some RMNs have been demonstrably attributed to crystallisation processes, where an RMN has crystallised from a melt; either in experimental studies (Schwander et al., 2015), or observed in cosmic spherules (Rudraswami et al., 2014). When these RMNs are superimposed over RMNs analysed in this study and the literature (Figure 9), crystallisation RMNs fall along the Fe mixing line and the high PGE region of the Ni mixing line. However, crystallisation RMNs also appear to extend into a region of low PGE and low Fe, which is not represented by any RMNs observed in meteorites. This presents a problem: if crystallisation was a dominant process in RMN formation we would expect this region of the graph to be populated with RMNs, which is not the case. Considering each element in isolation, overlaying crystallisation derived RMNs and modelled condensation curves over observed RMNs, from this study and the literature (Figure 10) reveals a further disparity. Although some observed RMNs do show some agreement with crystallisation derived RMNs in elements such as Rh, W, Pt and Ir (orange region), other elements such as Os, and particularly Mo, do not. Similarly, there are no distinct trends clustering around the condensation curves, except for

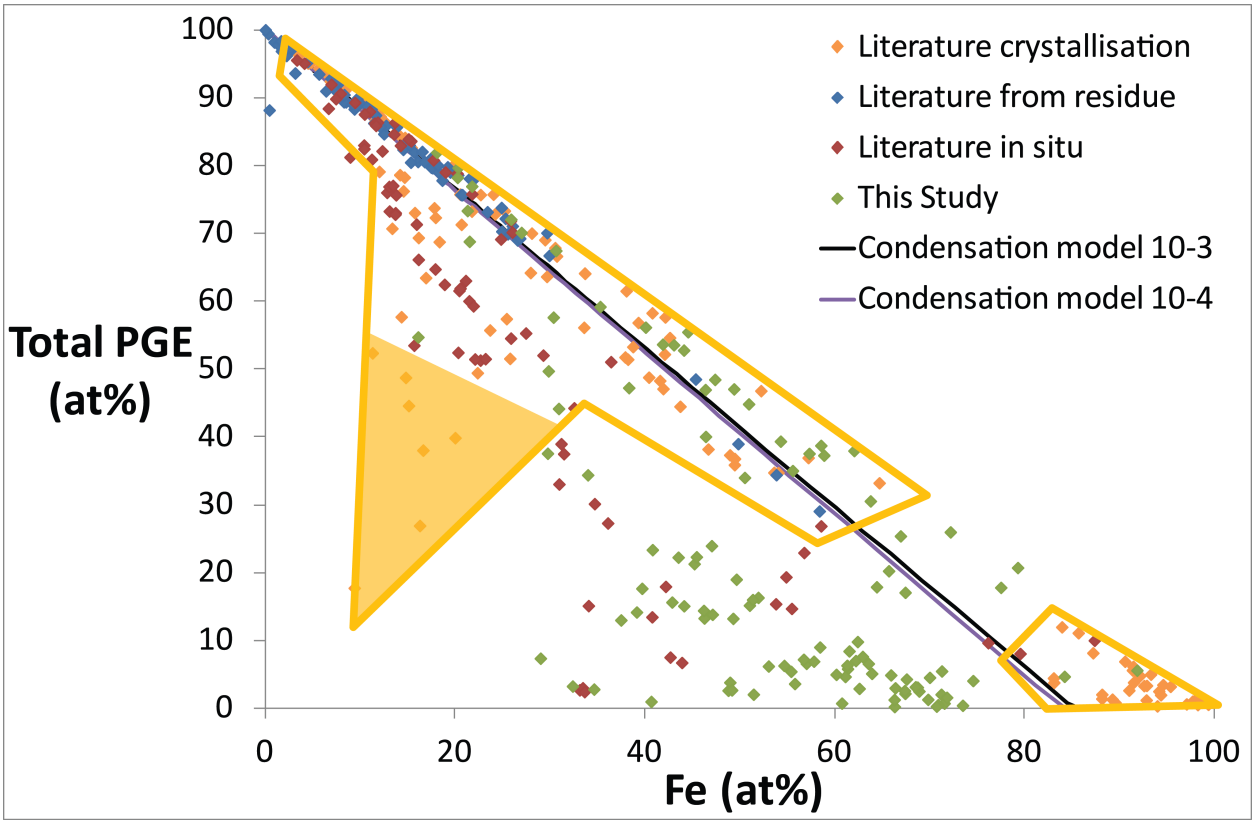

Figure 9: Total PGEs vs Fe for RMNs detailed in this study and the literature indicating the range of compositions that can be produced by crystallisation demonstrated by Schwander et al. (2015) andRudraswami et al. (2014)(orange region). The shaded region represents compositions that can be produced by crystallisation but are not observed in the RMN meteorite population

a weak association in Os, and Ir (blue region). Crystallisation encounters the same problem as condensation; whilst it can produce compositions consistent with some RMN observations, it cannot explain them all. Furthermore, the population of RMNs that are consistent with condensation and crystallisation are not complementary. Therefore, it cannot be an expression of both processes acting in tandem.

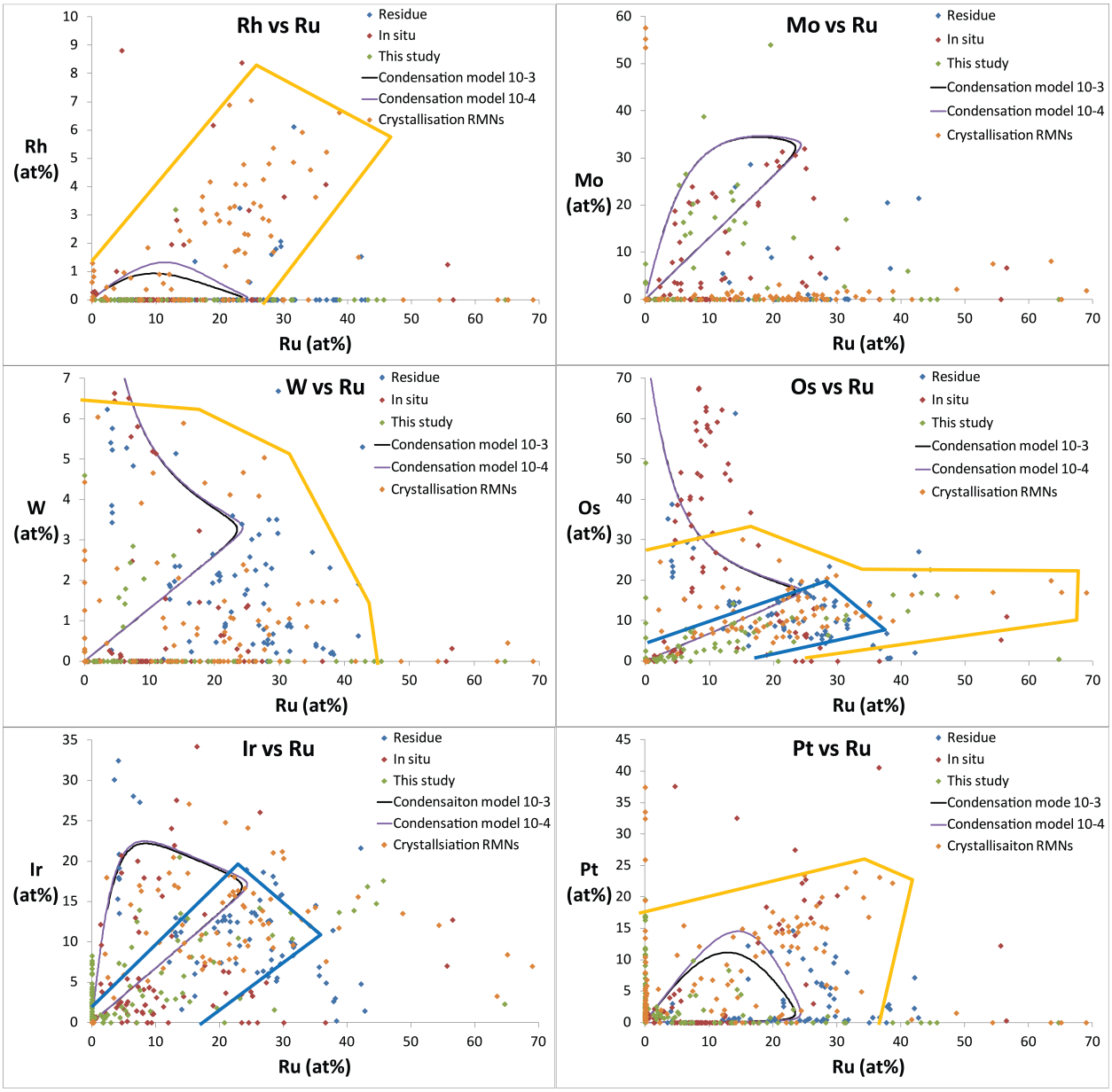

Figure 10: PGEs vs Ru comparing RMNs from this study and the literature with crystallisation derived RMNs and model condensation curves indicating very weak correlations for crystallisation in orange and condensation in blue.

4.3.4. Other parent body processes

To ascertain if there is any variation between RMNs from different parent bodies, RMNs were separated by meteorite (Figure 11). Allende seems to encompass the whole range of RMNs, however other meteorites

cluster into certain regions: Murchison Leoville, Orguiel, ALH 77307 and Adelaide represent certain portions of the Fe mixing line; Ornans follows the Ni mixing line into the low PGE region; and Vigarano contains RMNs from the low PGE region and the mid-section of the Fe mixing line.

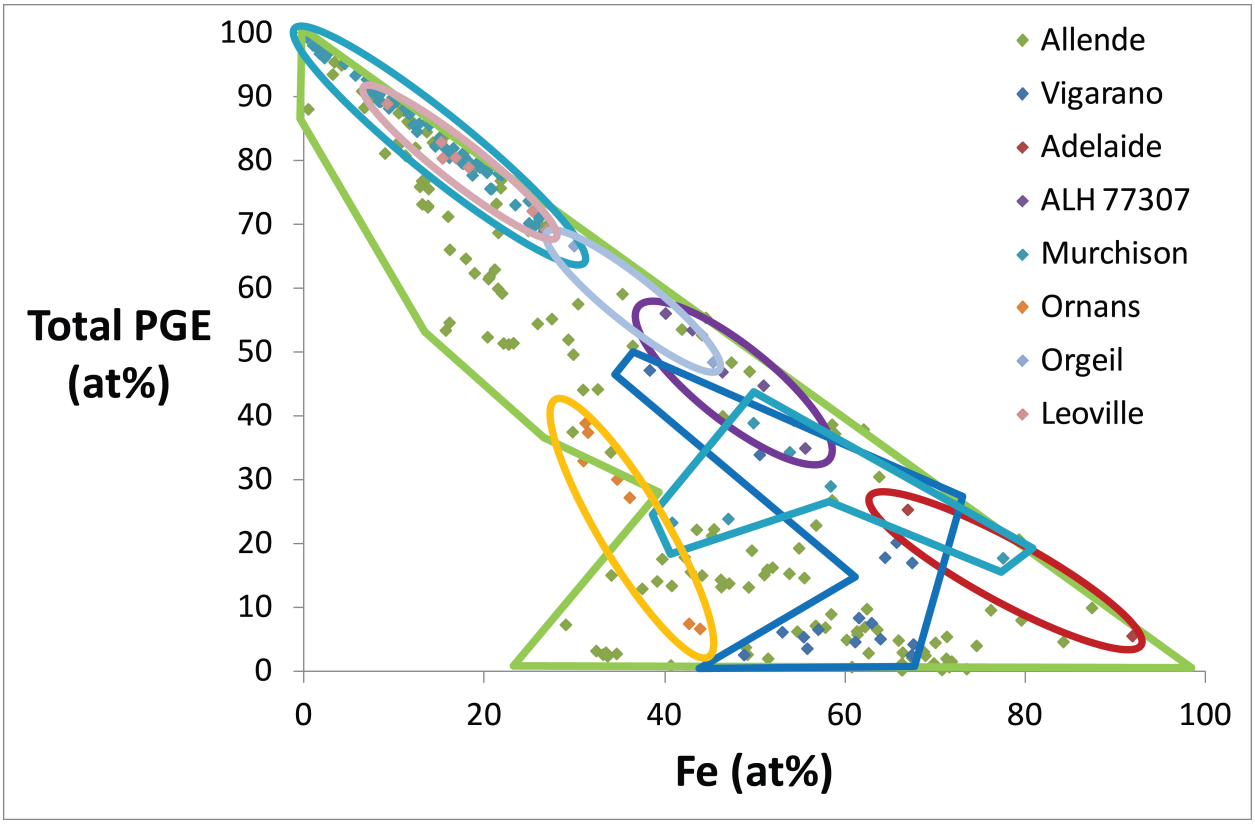

Figure 11: variability of total PGE vs Fe in RMN compositions across different meteorite hosts indicating a possible weak clustering of RMNs from Vigarano.

It is possible that this spread is due to a small data set for some meteorites. However, the methodology used in this study would find most, if not all RMNs in a thin section, and all observed RMNs were analysed. So we have to entertain the possibility that RMN populations may vary between parent bodies. In particular, the clustering of RMNs within Vigarano suggests this may be the case as several RMNs are observed and yet the spread of RMNs remains constrained.

PGEs are predominantly siderophile and generally unreactive with the exception of W and Mo which have been shown to be mobile under low degrees of alteration (Palme et al., 1998). To alter the PGE content in RMNs would require significantly higher temperatures than all carbonaceous chondrite parent bodies have experienced. However, Fe and Ni have siderophile and chalcophile tendencies and can be oxidised under certain conditions; in some cases RMNs have undergone sulphidation and oxidation. Therefore, RMN compositions could be altered by the removal or addition of Fe and/or Ni. These reactions are much easier to achieve at lower temperatures consistent with parent body alteration. However, the spread of RMN compositions is not consistent with regional metamorphism of RMNs which would create a narrow range

of RMN compositions as the elements are mobilised and redistributed around the parent body producing homogeneous RMN compositions. This leaves two possibilities: either RMNs have been altered by inhomogeneous localised alteration at the micron scale, or parent body processes have not affected the RMN population significantly.

4.3.5. Petrological context

Finally, one must take into account the context of the RMN. RMNs have been shown to occur throughout carbonaceous chondrites. The methodology described in this study retains their context and mineralogical association. Therefore, we can check if the formation process implied by evaluation of the chemical data is plausible. Indeed, it is the case that some RMNs with compositions consistent with a condensation origin are located within a mineral assemblage that has an igneous history, such as the RMNs in cosmic spherules from Rudraswami et al. (2014), and therefore cannot have a condensation origin. Furthermore, although crystallisation can produce a vast diversity of chemical compositions in RMNs, very few inclusions in meteorites have an igneous history. Therefore, most RMNs cannot have formed via this process.

4.3.6. An extra-solar initial origin?

We have to accept that neither condensation (primary nebula), crystallisation (secondary nebula), nor sulphidation (secondary asteroidal) and parent body processes can produce either individually or in tandem the myriad of compositions of RMNs we observe in meteorites. If we cannot produce the diversity of RMNs via a combination of nebular and/or parent body processes we are required to look elsewhere. The solar system formed from a giant molecular cloud fragment which would have included refractory metals from a variety of stellar sources. The resulting diversity of RMN compositions represents the initial condition of our protoplanetary disk. Our data indicates that while RMNs have been effected by condensation, crystallisation, sulphidation and (possibly other) parent body processes, none of these processes are dominant, and together, they have not homogenised the RMN population and the removed that initial compositional diversity. If this interpretation is correct, a prediction would be that pre-solar RMNs are present as discrete grains within primitively chondrites and IDPs (rather than solely hosted in pre-solar silicon carbide (Croat et al., 2013)), and that some of the grains analysed in the course of this study belong to that primordial population.

5. Conclusion

Observing RMNs in multiple components in meteorites, not just in CAIs, directly contradicts the assumption that RMNs are unique to CAIs. Each RMN host has its own characteristic RMN compositional suite. However, the average RMN composition across all minerals averages to the bulk solar system and CI chondrite implying that PGEs are primarily, if not uniquely, hosted within RMNs. Condensation models, experimentally derived RMNs from crystallisation, and parent body processes such as sulphidation are unable to produce the suite of RMN compositions observed, either in isolation or in tandem. The Solar

Nebula inherited a vast diversity of RMN compositions from a variety of stellar sources. Our data suggests that this initial RMN population was never fully homogenised: while some RMNs have been modified by nebular and asteroidal processes, the compositional diversity of the RMN population observed in this study indicates that the original primordial signature was never erased. If this assumption is correct, some RMNs may have escaped Nebular processing and will retain their primordial composition. Therefore, we should observe demonstrably primordial RMNs not just within pre-solar graphite, but in other components as well. These conclusions could only be drawn by analysis of RMNs *in situ* highlighting the importance of retaining context and petrological associations.

6. Acknowledgements

This work was funded by the Australian Research Council via their Australian Laureate Fellowship program. This research was undertaken on the XFM beamline at the Australian Synchrotron, Victoria, Australia. The authors acknowledge the facilities, and the scientific and technical assistance, of the Australian Microscopy & Microanalysis Research Facility at the Australian Centre for Microscopy and Microanalysis, the University of Sydney and the Centre for Microscopy, Characterisation and Analysis, University of Western Australia. The authors would also like to thank the rest of the Desert Fireball Network research group as well as Mr Timmons Erikson, Mr Mark Daly, Ms Mary Munroe, and Ms Sarah Hayes for their assistance.

7. References

Anders, E., Gros, J., Takahashi, H., Morgan, J., & Higuchi, H. (1975). Extinct superheavy element in the allende meteorite. *Science*, *190*, 1262–1271.

Berg, T., Maul, J., Schönhense, G., Marosits, E., Hoppe, P., Ott, U., & Palme, H. (2009). Direct evidence for condensation in the early solar system and implications for nebular cooling rates. *The Astrophysical Journal Letters*, *702*, L172.

Bischoff, A., & Palme, H. (1987). Composition and mineralogy of refractory-metal-rich assemblages from a ca, al-rich inclusion in the allende meteorite. *Geochimica et Cosmochimica Acta*, *51*, 2733–2748.

Blander, M., Fuchs, L., Horowitz, C., & Land, R. (1980). Primordial refractory metal particles in the allende meteorite. *Geochimica et Cosmochimica Acta*, *44*, 217–223.

Blum, J. D., Wasserburg, G., Hutcheon, I. D., Beckett, J. R., & Stolper, E. M. (1988). 'domestic'origin of opaque assemblages in refractory inclusions in meteorites, .

Campbell, A. J., Humayun, M., Meibom, A., Krot, A. N., & Keil, K. (2001). Origin of zoned metal grains in the que94411 chondrite. *Geochimica et Cosmochimica Acta*, *65*, 163–180.

Cleverley, J., Ryan, C., Hough, R., Bland, P., Fisher, L., & Dyl, K. (2012). Quantified, whole section, maia xrf mapping of trace elements in allende. *Meteoritics and Planetary Science Supplement*, *75*, 5175.

Connelly, J. N., Bizzarro, M., Krot, A. N., Nordlund, Å., Wielandt, D., & Ivanova, M. A. (2012). The absolute chronology and thermal processing of solids in the solar protoplanetary disk. *Science*, *338*, 651–655.

Croat, T., Berg, T., Bernatowicz, T., Groopman, E., & Jadhav, M. (2013). Refractory metal nuggets within presolar graphite: First condensates from a circumstellar environment. *Meteoritics & Planetary Science*, *48*, 686–699.

Dyl, K. A., Cleverley, J. S., Bland, P. A., Ryan, C. G., Fisher, L. A., & Hough, R. M. (2014). Quantified, whole section trace element mapping of carbonaceous chondrites by synchrotron x-ray fluorescence microscopy: 1. cv meteorites. *Geochimica et Cosmochimica Acta*, *134*, 100–119.

Eisenhour, D., & Buseck, P. (1992). Transmission electron microscopy of rmns: Implications for single-phase condensation of the refractory siderophile elements. *Meteoritics*, *27*, 217.

El Goresy, A., Nagel, K., Dominik, B., & Ramdohr, P. (1977). Fremdlinge: Potential presolar material in ca-al-rich inclusions of allende. *Meteoritics*, *12*, 215.

El Goresy, A., Nagel, K., & Ramdohr, P. (1978). Fremdlinge and their noble relatives. In *Lunar and Planetary Science Conference Proceedings* (pp. 1279–1303). volume 9.

Fegley, B., & Kornacki, A. S. (1984). The geochemical behavior of refractory noble metals and lithophile trace elements in refractory inclusions in carbonaceous chondrites. *Earth and planetary science letters*, *68*, 181–197.

Fegley, B., & Palme, H. (1985). Evidence for oxidizing conditions in the solar nebula from mo and w depletions in refractory inclusions in carbonaceous chondrites. *Earth and Planetary Science Letters*, *72*, 311–326.

Grossman, L. (1973). Refractory trace elements in ca-al-rich inclusions in the allende meteorite. *Geochimica et Cosmochimica Acta*, *37*, 1119–1140.

Grossman, L., & Ganapathy, R. (1976). Trace elements in the allende meteoritei. coarse-grained, ca-rich inclusions. *Geochimica et Cosmochimica Acta*, *40*, 331–344.

Grossman, L., Ganapathy, R., & Davis, A. M. (1977). Trace elements in the allende meteoriteiii. coarse-grained inclusions revisited. *Geochimica et Cosmochimica Acta*, *41*, 1647–1664.

Harries, D., Berg, T., Langenhorst, F., & Palme, H. (2012). Structural clues to the origin of refractory metal alloys as condensates of the solar nebula. *Meteoritics & Planetary Science*, *47*, 2148–2159.

Lodders, K. (2003). Solar system abundances and condensation temperatures of the elements. *The Astrophysical Journal*, *591*, 1220.

MacPherson, G., Simon, S., Davis, A., Grossman, L., & Krot, A. (2005). Calcium-aluminum-rich inclusions: Major unanswered questions. In *Chondrites and the protoplanetary disk* (p. 225). volume 341.

Palme, H., Borisov, A., & Wulf, A. (1998). Experimental determination of the oxidation sequence of refractory metals. In *Lunar and Planetary Science Conference* (p. 1611). volume 29.

Palme, H., Hutcheon, I., & Spettel, B. (1994). Composition and origin of refractory-metal-rich assemblages in a ca, al-rich allende inclusion. *Geochimica et cosmochimica acta*, *58*, 495–513.

Palme, H., & Wlotzka, F. (1976). A metal particle from a ca, al-rich inclusion from the meteorite allende, and the condensation of refractory siderophile elements. *Earth and Planetary Science Letters*, *33*, 45–60.

Palme, H., Wlotzka, F., Nagel, K., & El Goresy, A. (1982). An ultra-refractory inclusion from the ornans carbonaceous chondrite. *Earth and Planetary Science Letters*, *61*, 1–12.

Rudraswami, N., Prasad, M. S., Plane, J., Berg, T., Feng, W., & Balgar, S. (2014). Refractory metal nuggets in different types of cosmic spherules. *Geochimica et Cosmochimica Acta*, *131*, 247–266.

Ryan, C., Jamieson, D., Churms, C., & Pilcher, J. (1995). A new method for on-line true-elemental imaging using pixe and the proton microprobe. *Nuclear Instruments and Methods in Physics Research Section B: Beam Interactions with Materials and Atoms*, *104*, 157–165.

Ryan, C., Siddons, D., Kirkham, R., Dunn, P., Kuczewski, A., Moorhead, G., De Geronimo, G., Paterson, D., De Jonge, M., Hough, R. et al. (2010). The new maia detector system: methods for high definition trace element imaging of natural material. In *X-RAY OPTICS AND MICROANALYSIS: Proceedings of the 20th International Congress* (pp. 9–17). AIP Publishing volume 1221.

Schwander, D., Berg, T., Harries, D., Schönhense, G., & Ott, U. (2014a). Composition and clues to the origin of refractory metal nuggets extracted from chondritic meteorites. *Meteoritics & Planetary Science*, *49*, 1888–1901.

Schwander, D., Berg, T., Schönhense, G., & Ott, U. (2014b). Condensation of refractory metals in asymptotic giant branch and other stellar environments. *The Astrophysical Journal*, *793*, 20.

Schwander, D., Buhre, S., Schönhense, G., & Ott, U. (2015). Synthesis of refractory metal nuggets and constraints on the thermal histories of nugget-bearing ca, al-rich inclusions. *Meteoritics & Planetary Science*, *50*, 893–903.

Sylvester, P. J., Ward, B. J., Grossman, L., & Hutcheon, I. D. (1990). Chemical compositions of siderophile element-rich opaque assemblages in an allende inclusion. *Geochimica et Cosmochimica Acta*, *54*, 3491–3508.

Wänke, H., Baddenhausen, H., Palme, H., & Spettel, B. (1974). On the chemistry of the allende inclusions and their origin as high temperature condensates. *Earth and Planetary Science Letters*, *23*, 1–7.

Wark, D. (1986). Evidence for successive episodes of condensation at high temperature in a part of the solar nebula. *Earth and planetary science letters*, *77*, 129–148.

Wark, D., & Lovering, J. (1976). Refractory/platinum metal grains in allende calcium-aluminium-rich clasts (carc's): possible exotic presolar material? In *Lunar and Planetary Science Conference* (p. 912). volume 7.

Wark, D., & Lovering, J. (1978). Refractory/platinum metals and other opaque phases in allende ca-al inclusions. In *Lunar and Planetary Science Conference* (pp. 1214–1216). volume 9.